PROCEEDINGS, Thirty-Seventh Workshop on Geothermal Reservoir Engineering
Stanford University, Stanford, California, January 30 - February 1, 2012
SGP-TR-191

MECHANICAL PROPERTIES OF INTACT ROCK AND FRACTURES IN WELDED TUFF FROM NEWBERRY VOLCANO

Yawei Li, Jihoon Wang, Woodong Jung, Ahmad Ghassemi

Department of Petroleum Engineering, Texas A&M University
3116 TAMU 507 Richardson Building
College Station, TX, 77845, USA
E-mail: ahmad.ghassemi@pe.tamu.edu

ABSTRACT

In this paper we present the results of a testing program to characterize the rock mechanical properties of welded tuff from Newberry Volcano. The rock samples used in this work are four drill cores from the GEO-N2, GEO-N1, and Oxy-72 wells on the western flank of Newberry Volcano. Multistage triaxial compression tests were performed to determine Young's modulus, Poisson's ratio, and failure envelop. In addition, multistage triaxial shear tests were performed to determine the mechanical properties and shear strength of the fractures developed in triaxial compression tests. Joint roughness coefficient (JRC) and Joint Wall Compressive Strength (JCS) were obtained through back-analysis of the shear tests. It was found that the JCS of tested joints are larger than the intact rock Uniaxial Compressive Strength. The joint surfaces were characterized by a laser profilometer to correlate the surface roughness profile to the JRC from back-analysis of experimental data. Joint normal stiffness and shear stiffness were estimated and it was observed that a higher confining pressure results in higher joint shear stiffness. The stiffness is gradually reduced as the contact surfaces become smoother with additional shear displacement.

INTRODUCTION

In stimulation of an enhanced geothermal system (EGS), it is important to consider the fluid pathways between the injection and the production well(s), and the factors controlling them. The permeability of critically stressed fractures (CSFs) can be increased by reducing the effective stress through fluid injection. Critically stressed fractures are defined as pre-existing fractures that have slipped or are in the state of incipient slip because of the in-situ stress conditions. For the Newberry geothermal field, the primary permeability is extremely low; therefore, the secondary permeability (fractures, joints, etc.) must be used for heat exchange surfaces. This is achieved by water injection to create slip on joints to enhance permeability through dilation. Numerical simulation of this process is very important for reservoir development and post-injection data analysis. Therefore, the mechanical and hydraulic properties of intact rock and jointed rock are needed.

To obtain the required mechanical properties of intact rock and rock joints, it is necessary to measure the properties in the field or laboratory tests. Triaxial compression and shear tests are commonly used for determining the failure properties of intact rock and the friction properties of a jointed rock specimen, respectively. Several triaxial compression and shear tests were performed and the results are presented in this paper. The rock samples described herein include core plugs from the GEO-N2, GEO-N1 and Oxy-72 wells on the western flank of Newberry Volcano. These cores were taken from depths more than 4000ft from the surface.

TRIAXIAL COMPRESSION AND SHEAR TESTS

Laboratory compression test

Rock mechanical properties and failure criterion are mainly obtained from laboratory triaxial testing. The most widely used failure criterion is the Mohr-Coulomb criterion. To obtain the Mohr-Coulomb failure envelope, conventional triaxial testing is used. Conventional triaxial testing is simple but requires multiple samples. Aside from limited availability, multiple samples also provide potential uncertainty in the resulting parameters due to sample heterogeneity, as different samples might have significant variations in strength. The multistage triaxial test (Kovari and Tisa, 1975) resolves the uncertainty issue caused by heterogeneity. In this triaxial testing program a single sample is compressed at different confining pressures

and is subjected to deviator stress levels which do not cause irreversible or permanent damage. In each stage, a different confining pressure is used and the axial stress is increased via strain control until a predetermined stopping criterion is reached. The axial stress is decreased to the confining pressure and a new stage starts by applying a higher confining pressure. In the last stage, the sample is loaded until failure. The failure envelope can be estimated from the Mohr's circle resulting from the last loading stage and others obtained from the previous non-failure stages.

Different stopping criteria of the loading stage have been proposed by previous investigators, Kovari and Tisa (1975), Kovari et al. (1983), Kim and Ko (1979), Crawford and Wylie(1987). However their stopping criteria have two drawbacks: the sample can deform irreversibly or even fail before the stopping point is reached; the construction of failure envelope from a failure Mohr circle and the previous non-failure ones is not well-established and can be subjective. Tran et al (2010) proposed the use of volumetric strain deflection point (maximum contraction point) as the stopping criterion of axial loading in multistage triaxial test. This new termination point resolves the drawbacks of existing methods and is easy to pick. They have reported that the best fit tangent line of non-failure Mohr circles has the same slope as the failure envelope, thus the failure envelope can be obtained by moving up the non-failure envelope.

Laboratory shear test

Triaxial shear and direct shear test are used to determine joint properties. Generally these tests involve a constant normal stress and an increasing shear stress applied to the sample. Normal and shear stresses, as well as normal and shear displacement are recorded. Multistage testing refers to several tests undertaken at different normal stresses. The peak and residual shear strength can be estimated from the shear stress vs. shear displacement curve. A normal stress vs. shear stress curve can be drawn to demonstrate the shear strength characteristics of the discontinuity. Due to the difficulties in obtaining a sufficient number of identical samples, a single jointed sample is often used for multistage testing to extract the maximum information from a single sample. However, Barton (1973) reported that only low normal stress tests would provide reliable information on the peak strength characteristics of the discontinuity. Repeated shearing of the sample will crush the asperities and the rest of the test results fall somewhere between the peak and the residual values.

Joint Shear Criterion

The influence of joint roughness on its strength can be considered through the concepts of apparent friction angle and roughness coefficient (Patton, 1966):

$$\tau_p = \sigma \tan(\phi_\mu + i) \quad (1)$$

$$\tau_p = S_j + \sigma \tan(\phi_r) \quad (2)$$

Where Eqn. (1) is for small normal stress, Eqn. (2) for large normal stress, ϕ_μ is the friction angle of an ideally smooth joint surface, and i is the average asperities (teeth) inclination angle from the mean joint plane, ϕ_r is the residual friction angle when normal stress is larger than a critical normal stress. Actual data have shown a gradual transition from the initial slope at $\phi_\mu + i$ to the final slope at ϕ_r, because as the normal stress on the joint increases, it becomes easier to crush the asperity (teeth) rather than ride over them. Once the asperities are sheared, the joint friction angle is reduced to a new level namely, ϕ_μ (Fig. 1).

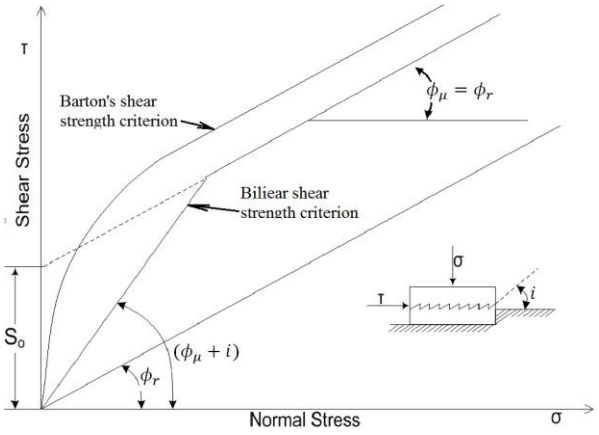

Figure 1: Barton's shear strength criterion and Patton's Bilinear shear strength criterion for an ideal asperity model of joint surface.

In addition to Patton's bilinear model, a number of empirical models have been proposed, such as the parabolic models of Jaeger (1971). More elaborate models taking into account the surface roughness and dilation were proposed by Landanyi and Archambault (1970), Barton (1973) and Barton and Choubey (1977). Of these, Barton's model is widely used:

$$\tau = \sigma_n \tan[JRC \log_{10}(\frac{JCS}{\sigma_n}) + \phi_b] \quad (3)$$

Barton's model contains two empirical parameters namely, JRC (joint roughness coefficient), and JCS

(joint wall compressive strength). The JRC (ranging from 0 to 20) is a dimensionless number that reflects the amount of surface undulations and asperities present in the discontinuity surface. The value of JCS is the normal stress at which the dilatancy contribution is reduced to zero and is taken as equivalent to uniaxial compressive strength. ϕ_b is the angle of shearing resistance mobilized at high normal stress levels at which all dilatancy effects are suppressed as all the asperities are sheared off forming a smooth shearing plane. It is characteristic of the rock mineralogy (Giani, 1992).

Estimation of JCS and JRC

JCS can be set equal to uniaxial compressive strength when the state of weathering of intact rock material and the joint walls is similar. Otherwise, the Schmidt hammer (Giani , 1992) technique is appropriate.

Barton and Choubey reported that JRC could be estimated through the back analysis of shear tests, where Eq. (3) is rearranged into the following form:

$$JRC = \frac{\arctan(\tau/\sigma_n) - \phi_b}{\log_{10}(JCS/\sigma_n)} \qquad (4)$$

They also described a residual tilt test in which pairs of flat sawn surfaces are mated and the pairs of blocks are tilted until slip occurs. Maerz and Franklin (1990) proposed a roughness characterizing method using shadow profilometer.

Estimation of ϕ_b

The basic friction angle can be estimated from direct shear tests on smooth joint, clean surfaces that have been prepared by diamond saw cut as recommended by Hoek and Bray (1981). The friction angle for most smooth unweathered rock surfaces lies between 25° and 35° (Barton and Choubey, 1977). A tilt test may also be used (Stimpson, 1981) by utilizing following equation:

$$\phi_A = tan^{-1}(1.155 tan\, \alpha_s) \qquad (7)$$

Where ϕ_A is the basic friction angle for the upper piece of core and as is the angle at which sliding commences.

Scale effects

There are significant scale effect in JRC and JCS (Barton and Choubey, 1977). As the joint length increases, joint wall contact is transferred to the larger and less steeply inclined asperities as the peak shear strength is approached, resulting in larger individual contact areas with correspondingly lower JCS and JRC values, causing a reduction in shear strength with size. Barton and Bandis (1982) proposed the following correction factors after undertaking extensive joint and joint replica testing and a literature review:

$$JRC_n \cong JRC_0 \left[\frac{L_n}{L_0}\right]^{-0.02JRC_0} \qquad (8)$$

$$JCS_n \cong JCS_0 \left[\frac{L_n}{L_0}\right]^{-0.02JRC_0} \qquad (9)$$

Where the subscripts ‘‘0’’ and ‘‘n’’ refer to laboratory scale (100 mm) and in situ block sizes, respectively. The JRC and JCS values used in Eqn. (3) refer to laboratory scale parameters (i.e., JRC_0 and JCS_0).

Joint Stiffness Characteristics

Joint stiffness parameters describe the stress-deformation characteristics of the joint and are fundamental properties in the numerical modeling of jointed rock. Usually they are measured in Direct Shear Test with joint displacement transducers. Usually they are measured in Direct Shear Test with joint displacement transducers. An indirect method using strain-gauge type extensometer in triaxial shear test can also be used (Rosso, 1976). Barton and Choubey (1977) suggested the following equation for the estimation of the peak shear stiffness (MPa/m):

$$K_s = \frac{100}{L_x}\sigma_n tan\left[JRC log_{10}\left(\frac{JCS}{\sigma_n}\right) + \phi r\right] \qquad (10)$$

where L_x is the joint length (m). The above equation assumes that the peak shear strength is reached after shearing approximately 1% of the joint length.

The joint normal stiffness (K_n) is the normal stress per unit closure of the joint. It is influenced by the initial actual contact area, joint wall roughness, strength, deformability of the asperities, and properties of infill material (Bandis et al. 1983).

PETROLOGIC DESCRIPTION OF CORE SAMPLES

Petrographic thin section images were prepared for the description of N1-4013 samples (Fig.2). As Fig. 3 shows, N1-4013 sample has a porphyritic to aphanitic texture and is intermediate in composition between porphyritic rhyolite and aphanitic andesite. The rock is a dacite, or lithic tuff with pre-dominantly andesitic composition with glassy light gray matrix. This tuff contains micro-porphyritic feldspar, quartz, and small amount of amygdales, green smectite/clay and zeolite. A pre-existing vertical fracture (healed) is observed in N-4013-1H sample.

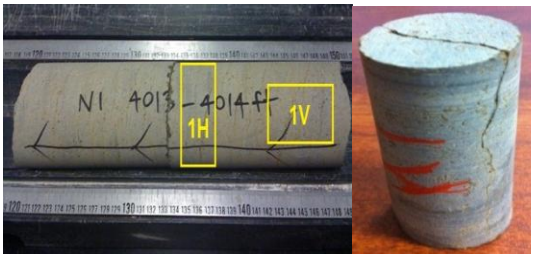

Figure 2: drilled core N1 from 4013-4014 feet depth showing the location of the plugs; Core plugs of N1-4013-1H before triaxial tests.

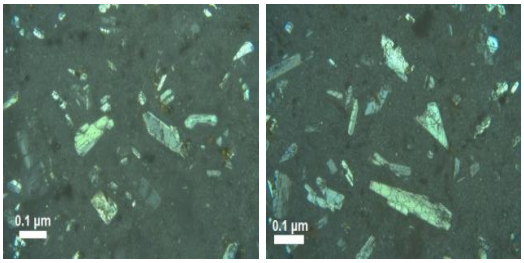

Figure 3: Petrographic images of core plugs N1-4013-1H and N1-4013-1V (right). Views are under crossed polarizers.

Figure 4: drilled core N1 from 4348-4349 feet depth showing the location of the plugs; Core plug of N1-4348-2H before triaxial tests.

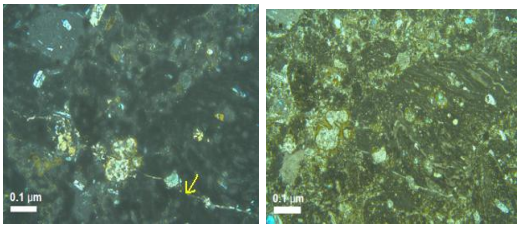

Figure 5: Petrographic images of core plug N1-4348-2H. Views are under crossed polarizers and plain light (right).

Core N1-4348-4349 (Fig. 5) has an aphanitic texture and is intermediate in composition between porphyritic rhyolite and aphanitic andesite. It is an intermediate tuff or rhyolite tuff, containing massive microcrystalline to cryptocrystalline minerals. The rock also contains bright colored fragments that are plagioclase minerals within a buff color clay matrix. The high clay content suggests ductile behavior; however, brittle behavior might also be present because of fine-grained and large crystals. In addition, small-sized vesicles are observed (blue color on the thin sections). A pre-existing fracture is shown in Fig. 5 (Yellow arrow) and is filled with calcite.

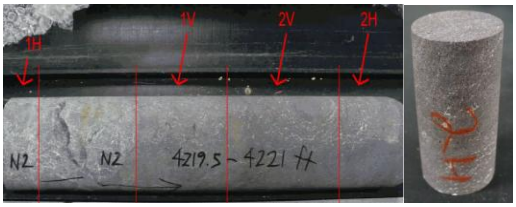

Figure 6: drilled core N2 from 4219 feet depth showing the location of the plugs; Core plug of N2-4219-2H before triaxial tests.

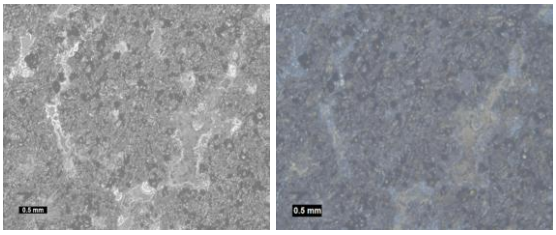

Figure 7: Thin section images of N2-4219. Views are under crossed polarizers.

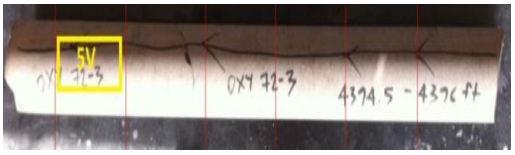

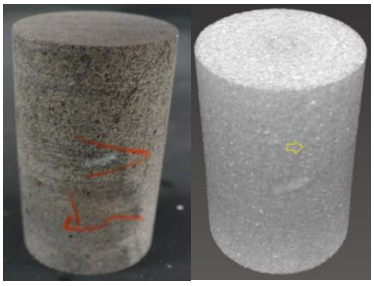

Figure 8: a drilled core OXY 72-3, from 4394.5-4396 feet depth; core plug OXY-5V and its 3D CT image prior to testing.

The lithology of the core sample *N2-4219* ranges from basaltic to andesitic in nature, consisting of plagioclase and quartz. The majority of the secondary minerals filling the non-clay fractures are silica and calcite.

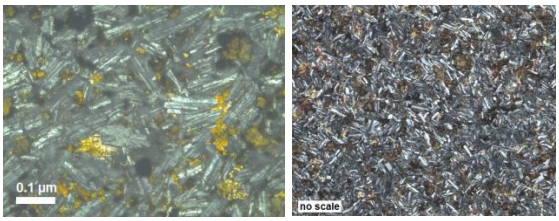

Figure 9: Petrographic images of the core plug OXY-5V. Views are under crossed polarizers.

The plug OXY-5V has an aphanitic fine-grained texture (Fig. 9). I t is a mafic igneous basalt, with dominantly plagioclase (light-colored), and dark gray minerals (possibly iron-oxide minerals) with minor hematite. It is expected that the rock is rather brittle. A pre-existing healed fracture is observed in Oxy-5V sample.

EXPERIMENTAL PROCEDURES, RESULTS AND INTERPRETATIONS

The specimens were first fully saturated with water using a vacuum pump prior to being jacketed to isolate it from the confining oil. All the samples have standard 1"×2" cylindrical shape. Four multistage triaxial compression tests were carried out to determine the mechanical properties and four Mohr-Coulomb failure envelopes; then four multistage triaxial shear tests were conducted to determine the frictional shear strength of the newly formed fractures/joints.

Multistage Triaxial Compression Tests

Each test has five different pressure stages; in the last stage, samples are compressed to failure to induce a macroscopic fracture. The axial stress was applied using a strain control mode at a rate of 7×10-6 strains/sec. Before the deviatoric loading was increased, the strain gauge readings were nulled at 50 psi of deviator stress. The following procedure is followed:

(i) The sample is subject to the first confining pressure (hydrostatical condition).
(ii) Axial load is applied by strain rate ($7x10^{-6}$/sec) control at constant confining pressure. Axial, lateral, and volumetric strains are recorded continuously.
(iii) The stage is over when the deflection point of the volumetric strain curve is reached ($d\varepsilon_v / d\sigma=0$).

The axial load is slowly brought back to the confining pressure and the process is repeated for a new stage. Figs. 10 and 11 show the stress-strain curves for two of the samples. For the non-dilatant specimen (N1-4348-2H), the stopping point was where the tangent modulus ($d\sigma/d\varepsilon_x$) decreases more than 2% from the linear portion of the curve. We assume that the ratio of ultimate strength to the stress at 2% tangent modulus deviation is constant for every pressure stage, the ratio can be determined in the last stage, thus the strengths of previous non-failure stages can be inferred with this ratio.

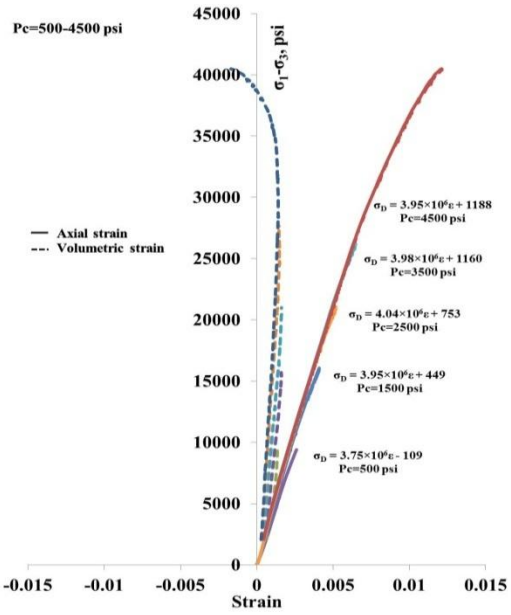

Figure 10: Stress-strain response at 5 stages of N1-4013-1H.

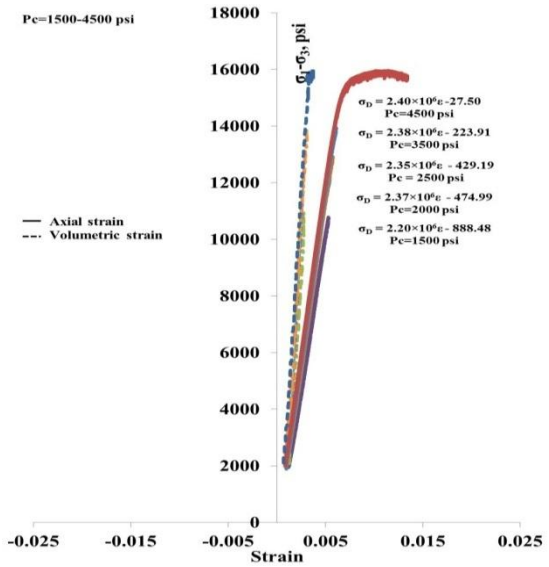

Figure 11: Stress-strain response at 5 stages of N1-4348-2H.

Figure 12: the four samples after compression test, N1-4013-1H, N1-4348-2H, N2-4219-2H, Oxy-5V.

We determined the failure envelope for each sample by assuming that the best fit tangent line of non-

failure Mohr circles has the same slope as the failure envelope, as shown in Fig. 13.

The results of the compression test are summarized in Table 1. It can be seen that the Oxy-4395-5V is much stronger than N1 and N2 samples, and has a larger elastic modulus; although there are pre-existing fractures in N1-4013-1H and Oxy samples, they still have higher strength and modulus than other two samples. The uniaxial compressive strengths, cohesions, internal friction angles obtained here are comparable to those published by Lutz et al. (2010). It was found that shear fractures induced in compression tests intersect the pre-existing fractures

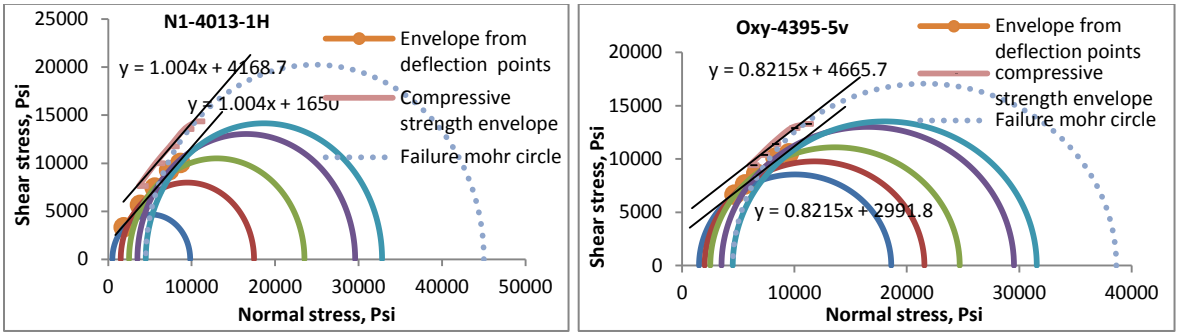

Figure 13: failure envelope construction of N1-4013-1H and Oxy-4395-5V.

Table.1 mechanical properties obtained from compression.

	N1-4013 (1H)	N1-4348 (2H)	N2-4219 (2H)	Oxy-4395 (5V)
Young's Modulus(psi); Poisson Ratio	3,945,273; 0.42 (Pc=4500 psi)	2,402,227; 0.28 (Pc=4500 psi)		6,822,836; 0.41 (Pc=4500 psi)

UCS, psi	17,676	10,811	8,270	17,247
Cohesion, psi	3,586	3,376	2,211	3,955
Friction angle	45.1^o	26.3^o	33.8^o	39.1^o

Multistage Triaxial Shear Tests

Four multi-stage shear tests were performed on the four compression-induced jointed rock samples.

Figure 14: sample (fractured tuff) assemble ready for multistage triaxial joint shear test.

One multi-stage triaxial shear test usually consist of 6-9 stages, one stage has one constant confining pressure. The following experimental procedure is followed:

(iv) The sample is pressurized (hydrostatically) to the first confining pressure.

(v) Axial load is increased via strain rate (7e-6/sec) control at constant confining. Axial, lateral, and volumetric strains are recorded continuously.

(vi) The stage is over when the joint surfaces begin to slip, the deviator stress ceases to increase, the stress-strain curve become flat.

(vii) The axial load is immediately decreased back to the confining pressure (hydrostatic).

(viii) The confining pressure is increased to the next value.

(ix) Steps (ii) to (v) are repeated for as many stages as required.

For the four tested samples, the used confining pressures of every stage are enumerated in Table.1

Table 2: confining pressures used during four multi-stage triaxial shear tests

Sample / Stage Pc (psi)	N1-4013 (1H)	N1-4348 (2H)	N2-4020 (2H)	Oxy-4395 (5V)
1	200	200	200	200
2	500	500	500	500
3	730	730	730	730
4	1020	1020	1020	1020
5	1450	1450	1450	1450
6	3200	3000	2176	4500
7	5500	4500	4500	6200
8			6100	

There are usually 3 confining pressures from 0 to 1000 psi, this is to better illustrate the gradual transition from the initial slope at $\phi_\mu + i$ to the final slope at ϕ_r of the shear strength envelope of joint, the more stages one has from 0 to 1000Psi, the clearer the transition is. Test data is then used to develop shear strength envelop for the joint. The shear strength of the jointed specimen is determined by constructing Mohr circles for each stage of the test in the normal stress vs. shear stress domain. The failure inclination angle θ is pre-determined and is used to calculate the stresses on the failure plane for each stage (Goodman, 1989).

INTEGRATION OF COMPRESSION AND SHEAR STRENGTH ENVELOPES

With the strength data of a multi-stage triaxial shear test, one can obtain the shear strength envelope of a jointed sample in normal-shear stress domain, together with the compressive (intact) strength

envelope, as shown in Fig. 15.

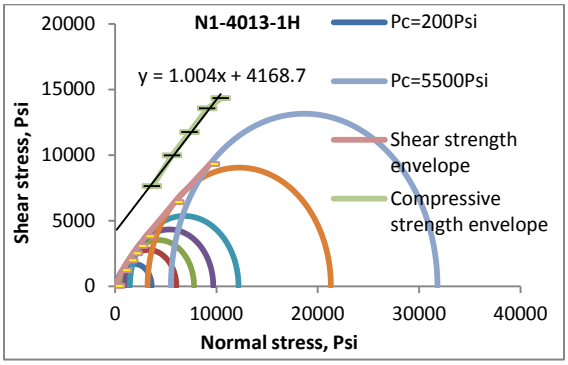

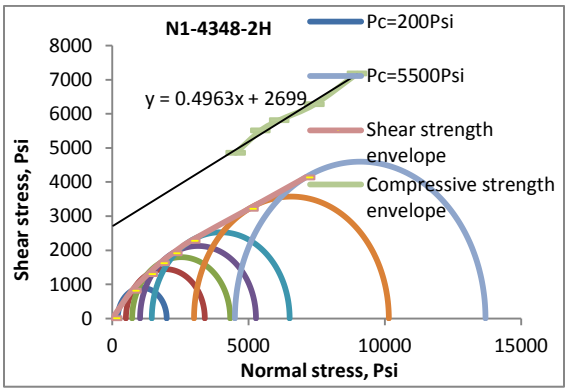

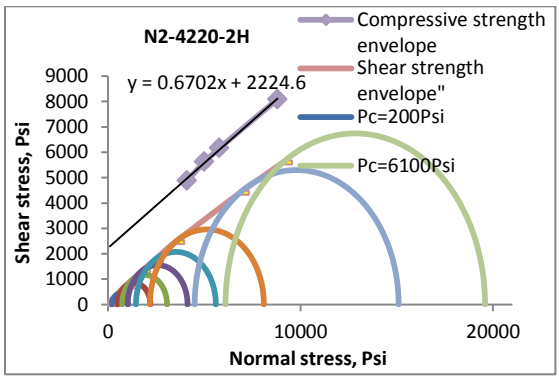

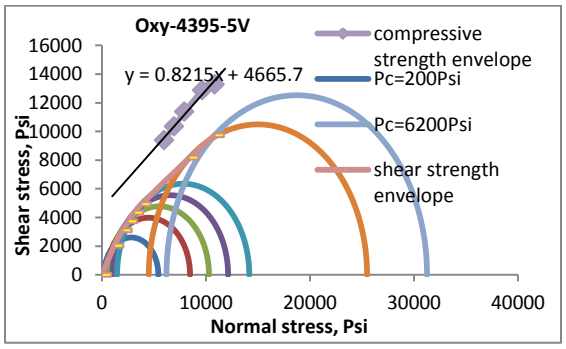

Figure 15: intact rock compressive strength envelope and shear strength envelope and Mohr circles of shear test.

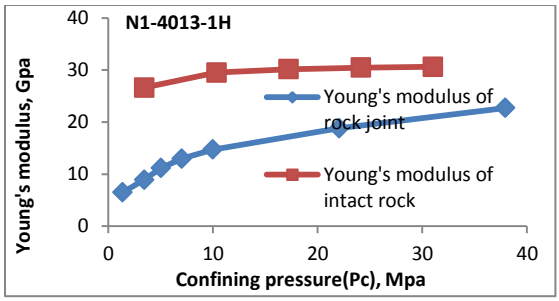

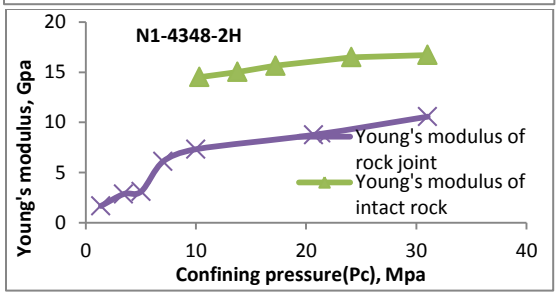

Figure 16: Young's modulus degradation from the intact rock to the jointed rock because of joint closure.

With a shear strength envelope, the JRC, JCS and ϕ_b in Barton's shear strength model can be determined through back-analysis, a least-square curve fitting method is used to determine the three parameters of a shear strength envelope, the equivalent friction angle of any point on Barton's JRC-JCS curve can be obtained by taking the inverse tangent of Barton's curve slope, as shown in Fig. 17. Similarly, the other shear strength envelopes are processed and the results are summarized in Table 3. As it can be seen in Table 3, the residual friction angles are smaller than the internal friction angles, because the asperities were sheared off after the repetitive shear tests; the fracture surfaces are smoother than the newly formed fracture surfaces.

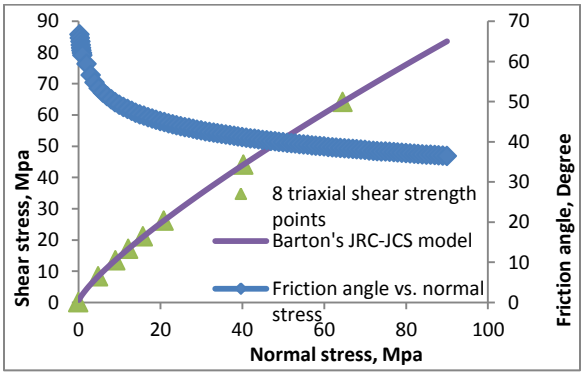

Figure 17: the 8 joint shear strength points, Barton's model curve and friction angle trend, N1-4013-1H.

Table 3: summary of frictional angles and Barton's model parameters.

Sample ID	Internal friction angle	$\phi_\mu + i$ (σ_n=0)	ϕ_b (ϕ_r)	i	JRC	JCS MPa	UCS inferred MPa
N1-4013-1H	45.1°	66.7°	38.5°	28.3°	0.236	188.8	140.1
N1-4348-2H	26.3°	60.0°	19.2°	40.8°	0.353	170.2	60.3
N2-4020-2H	33.8°	47.6°	28.5°	19.1°	0.127	181.3	57.6
Oxy-4395- 5V	39.1°	53.7°	32.9°	20.8°	0.372	196.9	122.2

JOINT STIFFNESSES FROM MULTISTAGE SHEAR TEST

The procedure proposed by Rosso (1976) is used for determining the joint stiffness using the test result of the multistage triaxial shear test and the results are shown in Fig. 18-21 (Table 4).

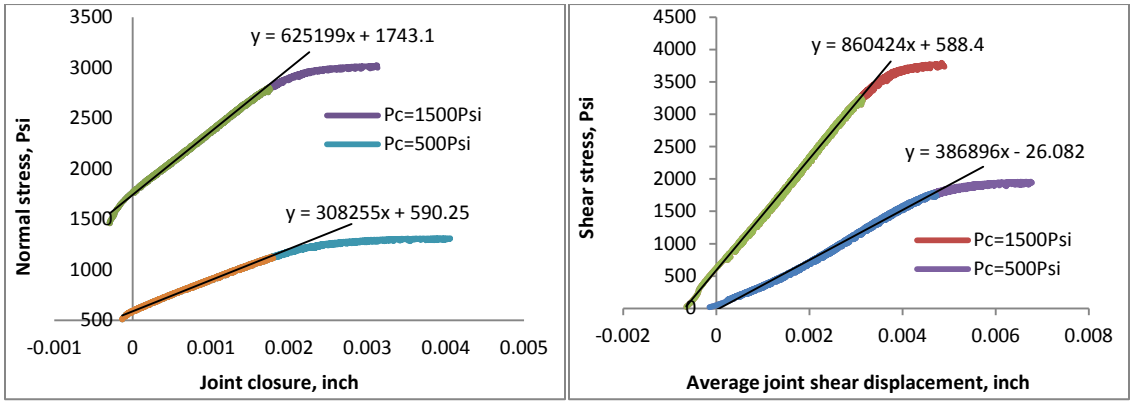

Figure 18: normal and shear stiffness of N1-4013-1H.

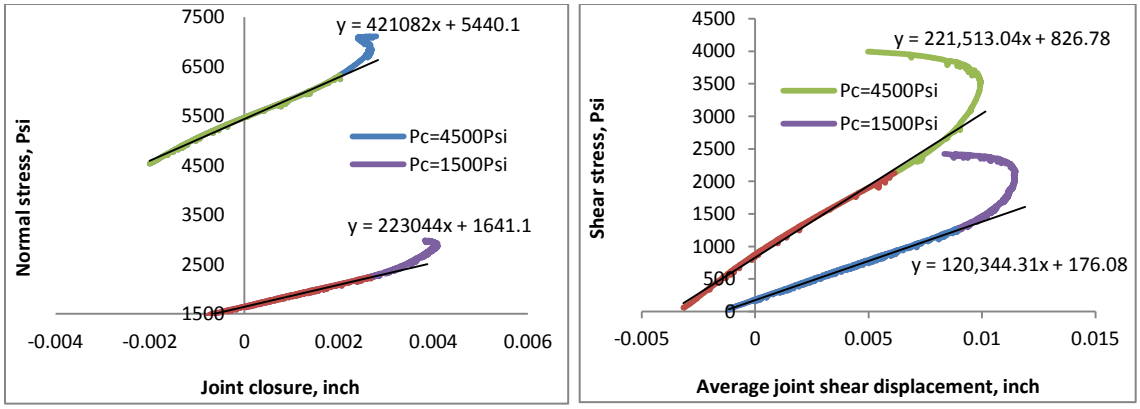

Figure 19: normal and shear stiffness of N1-4348-2H

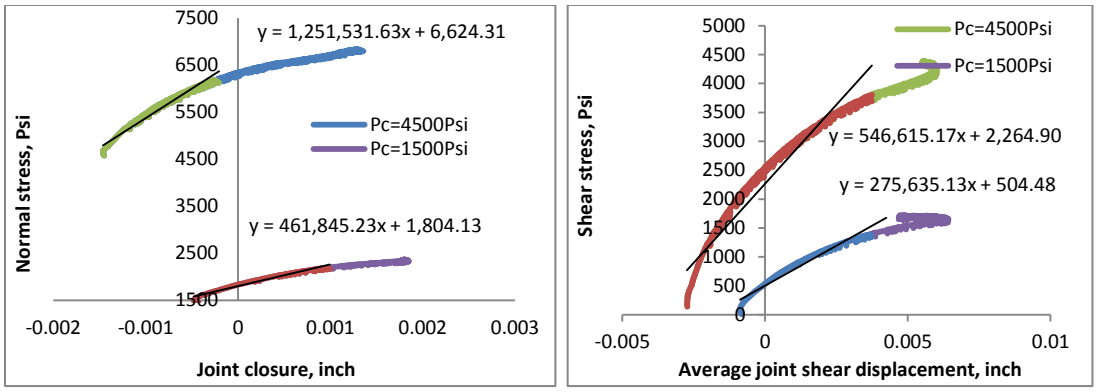

Figure 20: normal and shear stiffness of N2-4020-2H.

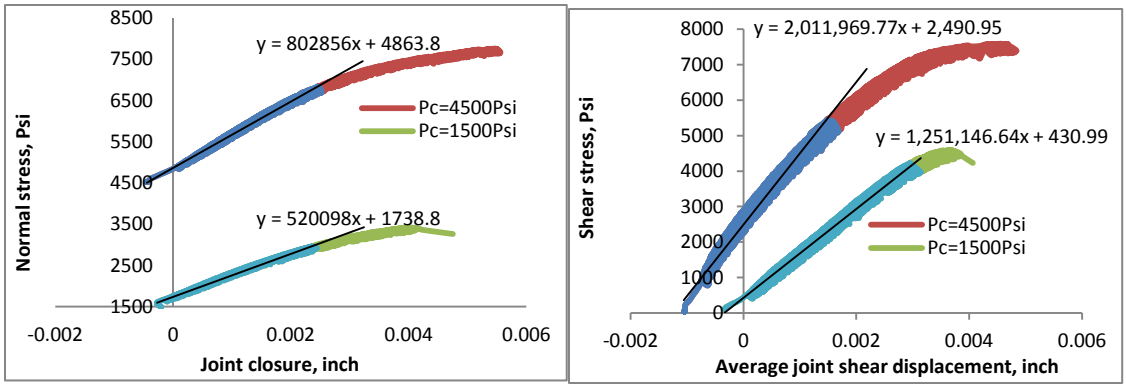

Figure 21: normal and shear stiffness of Oxy-4395-5V.

Table4: Summary of stiffness values.

Pc, psi	K_n & K_s(psi/in)	N1-4013-1H	N1-4348-2H	N2-4020-2H	Oxy-4395- 5V
500	K_n	308255	×	×	×
	K_s	386896	×	×	×
1500	K_n	625199	223044	461845	520098
	K_s	860424	120344	275635	1251146
4500	K_n	×	421082	1251531	802856
	K_s	×	221513	546615	2011969

JOINT SURFACES CHARACTERIZATION BY LASER PROFILER

The surface roughness of joints has critical influence on the shear behavior. It is necessary to evaluate the surface roughness directly using surface profiling tools. In this work, the surface roughness is measured after shear tests using a non-contact type of joint roughness measurement system (laser displacement gauge) as shown in Fig. 22. One pairs of joint surfaces are scanned and the profiles are compared to a set of published standards of Barton (Fig. 23). It was found that for similar profiles, the JRC value obtained from back-analysis is much smaller than that of the Barton's standard profile.

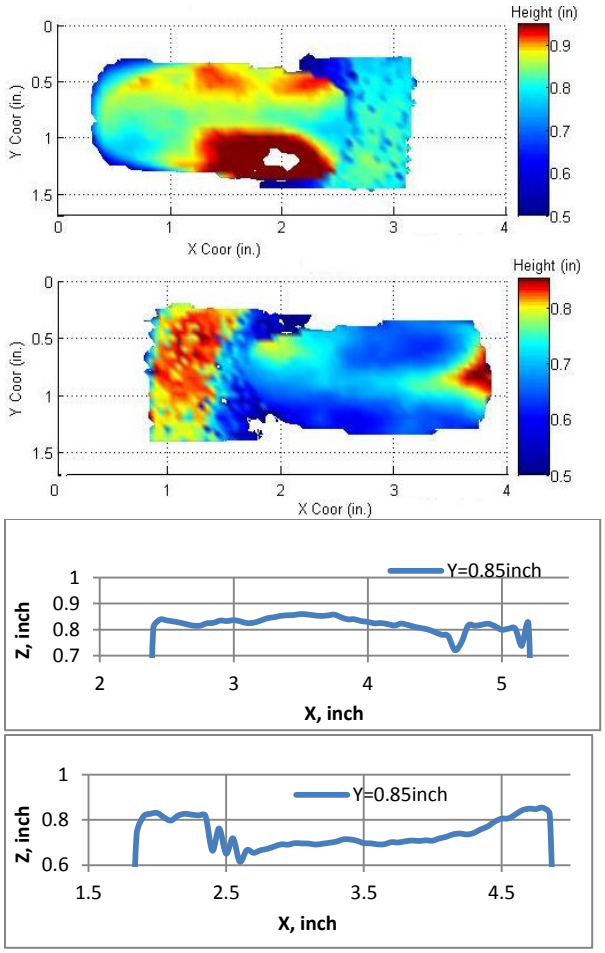

Figure 22: surface roughness profile of two fracture surfaces, N2-4220-2H.

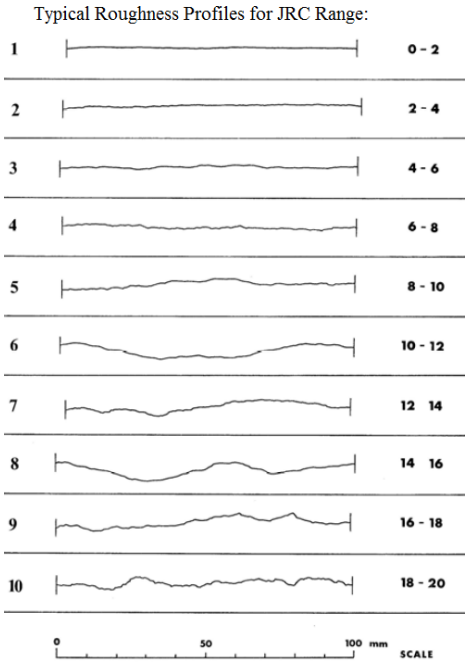

Figure 23: Barton's standard surface roughness profile.

DISCUSSION AND CONCLUSION

Multi-stage triaxial tests have been successfully performed on drill cores from GEO-N2, GEO-N1, and OXY-72-3 wells and on the flank of Newberry Volcano. The results have been used to determine the strength and failure properties of different lithofacies observed in the cores. Petrological analysis and mineralogical compositions of tuffs correlate with their mechanical properties, samples with more clay content show low strength; fine-grained siliceous sample (Oxy-5v) is stronger than the courser-grained samples. Brittle behavior with high dilatancy has been observed in the basaltic samples. The clay-rich interval (N1-4348-4349) displays a strongly ductile deformation. Extensive zones of ductile lithology ought to be avoided in stimulation design. Pre-existing closed fractures are prevalent in the basaltic samples and they are intersected by the compression induced fractures at failure. This indicates that the pre-existing fractures have very large shear strength and/or are not critically oriented in the specimen. The samples fractured in triaxial compression tests were then used in multi-stage joint tests to determine the natural fracture properties of the lithofacies. Joint stiffness and Barton joint model parameters were determined from the experimental results. The JRC values from back-analysis are much smaller than the value from visual comparison with Barton's standard JRC. We postulate that water might influence the shearing process, make the JRC values smaller, a shear test on a dry fracture might give higher JRC values. Repetitive shearing of one fractured sample crushes the asperities and makes the fracture surface smoother, thus the friction angle is reduced. The JCS values are larger than the uniaxial compressive strength which might be attributed to size effect. The surface roughness of newly formed joint is not profiled in this study, a comparison between the roughness before and after shear test will give us more insight in asperity damage (shearing off). More detailed investigations are needed to resolve the above-mentioned data uncertainties.

REFERENCES

Barton, N. (1972), "A model study of rock-joint deformation." *Int J Rock Mech Min Sci Geomech Abstr;* 9:579–602.

Barton, N. (1973), "Review of a new shear strength criterion for rock joints," *Engineering Geology*, 7:287–332.

Barton, N., Bandis S. (1982), "Effects of block size on the shear behavior of jointed rock," *23rd US Symposium on Rock Mechanics, Berkeley, CA*,. p. 739–60.

Barton, N., Bandis S. (1990), "Review of predictive capabilities of JRC-JCS model in engineering practice," In: Barton N, Stephansson O, editors. *Proceedings of the International Symposium on Rock Joints*, Loen, Norway. Rotterdam: Balkema,. p. 603–10.

Barton, N., and Choubey,V. (1977), "The shear strength of joints in theory and in practice," *Rock Mech.*, vol. 10, pp. 1-65.

Brown, W. S. & Swanson S. R. (1972), "Laboratory study of rock joint strength and stiffness under confining pressure," *Air Force Weapons Laboratory Final Report No, F29601-71-C-0050*.

Crawford, A., and Wylie, D. (1987), "A modified multiple failure state triaxial testing method," *28th US Rock Mechanics Symposium*, 133-140.

Tran, D.T., Pagoulatos, A., Sonderge, C.H. (2010), "Quantify Uncertainty of Rock Failure Parameters From Laboratory Triaxial Testings Using Conventional And Multistage Approaches," *44th U.S. Rock Mechanics Symp., June 27 - 30, 2010, Salt Lake City, Utah*

Giani, G.P.(1992), "Rock slope stability analysis," Rotterdam: A.A Balkema Publishers.

Goodman, R.E, (1989), "Introduction to Rock Mechanics, 2nd Edition"

Hoek, E, Bray, J.W. (1981), Rock slope engineering, 3rd ed. London: Institute of Mining and Metallurgy.

Jaeger, J.C. (1971). "Friction of Rock and Stability of Rock Slopes," *Geotechnique*, 21 (2):97-134.

Kim, M. M., and H. Y. Ko.(1979), "Multistage triaxial testing of Rocks," *Geotechnical Testing* 2: 98-105.

Kovari, K., Tisa, A., Einstein, H., and Franklin, J.A. (1983), "Suggested methods for determining the strength materials in triaxial compression," *Int. J. of Rock Mech. & Min. Sci. & Geomechs Abs.* 20: 283-290.

Landanyi, B. and Archambault, G. (1970) "Simulation of the shear behavior of a jointed rock mass," *11th Symposium on Rock Mechanics, American Inst. Min. Met. Petr. Engineers*, New York, pp 105-125.

Maerz, N.H, Franklin, J.A., and Bennett, C. P. (1990), "Joint roughness measurement using shadow profilometry," *Int. J. Rock Mech. Min. Sci.*, 27(5), 329–343.

Patton, F. D. (1966), "Multiple modes of shear failure in rock," *Proc. 1st Int. Cong. Int. Soc. Rock Mech., Colouste Gulbenkian Foundation, Lisbon*, vol. 1, pp. 509-513.

Rosso, R.S. (1976), "A comparison of joint stiffness measurements in direct shear, triaxial compression and in situ." *Int. J. Rock Mech. Min. Sci. & Geomech. Abstr*., 13:167-172

Stimpson, B. (1981), "A suggested technique for determining the basic friction angle of rock surfaces using core," *Int J Rock Mech Min Sci Geomech Abstr;*18:63–5.

Wawersik, W. R. (1974), "Deformability and strength of singly and multiply jointed sandstone in quasi-static compression." *Defense NuclearAgency Contract No. DNA001-73-C-0034.*